Determining of the composition of the metallic core of historical objects from surface XRF spectrometry data

Spectrochimica Acta Part B: Atomic Spectroscopy 220 (2024) 107030

Contents lists available at ScienceDirect

Spectrochimica Acta Part B: Atomic Spectroscopy

journal homepage: www.elsevier.com/locate/sab

Determining of the composition of the metallic core of historical objects from surface XRF spectrometry data

Antonio Doménech-Carbó [a,*], Marianne Mödlinger [b,*], Giorgia Ghiara [c]

[a] Departament de Química Analítica, Universitat de València, Dr. Moliner, 50, 46100 Burjassot, València, Spain
[b] Institut für Archäologien, Universität Innsbruck, Innrain 52A, 6020 Innsbruck, Austria
[c] DISAT, Politecnico di Torino, Corso Duca degli Abruzzi 24, 10129 Torino, Italy

ARTICLE INFO

Keywords:
Archaeometry
Metal composition
Portable XRF
Brass

ABSTRACT

A method for estimating the composition of the metal core in historical and archaeological artifacts using surface X-ray fluorescence (XRF) data is described. The method is based on the combination of fluorescence data recorded at points of the object with different degrees of corrosion exploiting the general phenomenon of demetallation of the less noble components of the metal alloy. A theoretical approach is provided using the Johnson–Mehl–Avrami–Erofeev-Kolmogorov (JMAEK) formalism to describe demetallation. Experimental data for binary Zn—Cu brass and Pb- and Sn-containing brass from Hofkirche in Innsbruck agree satisfactorily with the model.

1. Introduction

The determination of the composition of metallic nuclei is one of the most important analytical objectives in archaeometallurgy [1,2]. Due to the availability of portable instruments, X-ray fluorescence spectrometry (XRF) is a reference technique for the non-invasive analysis of valuable metal objects [3,4]. However, because the metal surface is usually covered by layer(s) of corrosion and patination, quantitative XRF results are usually less reliable in determining the composition of the metal core [5,6]. In such cases, samples representative of the bulk alloy must be taken which severely limits the analytical process.

The performance of portable XRF spectroscopy depends on the ability of the fluorescence signal to penetrate relatively shallow corrosion layers. Depending on the energy of the radiation and the composition of the corrosion layers, this technique provides an average elemental composition of a region whose thickness is in the range of microns to tens of microns [7,8]. This means that, under normal conditions, XRF does not provide direct information about the composition of the core of metallic objects.

In this context, considerable efforts have been made to test the reproducibility of the measurements [9,10], prepare certified reference materials [11,12], develop signal refinement methods [13], and chemometric tools for statistical data analysis of signal [14,15]. The purpose of the present work is to describe a simple graphical/algebraic method applicable to surface XRF data, for estimating the composition of the metallic core of corroded metallic objects. The method is based on the influence of concentration gradients existing in corrosion layers due to selective de-metallation processes on the elemental composition of such layers, in particular, dezincation in brass [16,17]. Here, such processes are studied within the theoretical framework of solid state reaction kinetics, resulting in a satisfactory modeling of XRF data using Johnson-Mehl-Avrami-Erofeev-Kolmogorov (JMAEK) based Eqs. [18]. The method is applied to a series of 18 brass statues from the Hofkirche in Innsbruck, Austria, fabricated in different workshops between 1509 and 1550. These were already studied in their historical context continuing previous archaeometric studies [19–21].

2. Experimental

Data for 18 Renaissance brass statues from the Hofkirche in Innsbruck, Austria. Surface XRF data. Surface XRF data were acquired with a portable ED-XRF analyzer (model: X-MET5100) from Oxford Instruments. In all cases, XRF measurements were taken on areas where the corrosion layers are visually uniform The analyzer is equipped with a high-resolution detector 45 kV Rh target X-ray tube with max. Current 50 μA. The measurement conditions used were voltage 40 kV, current 10 μA, and acquisition time 60 s. The spot measurements had a diameter of approximately 9 mm.

* Corresponding authors.
E-mail addresses: antonio.domench@uv.es (A. Doménech-Carbó), marianne.moedlinger@gmail.com (M. Mödlinger).

https://doi.org/10.1016/j.sab.2024.107030
Received 20 February 2024; Received in revised form 19 August 2024; Accepted 21 August 2024
Available online 24 August 2024

3. Results and discussion

Let us consider a metallic object large enough to allow surface XRF measurements to be taken over several areas of its surface. If a compositionally homogeneous object has suffered non-homogeneous corrosion (or if the composition of the base metal is heterogeneous), the surface XRF measurements will give different compositions for the different areas. In most cases, the corrosion process involves the selective removal of metals from the surface. This creates a concentration gradient between the surface and the inner layers of the corrosion region. This process will be faster for the less noble metal (typically, Zn in brass) whose concentration will be significantly reduced from the core of the metal to the outer region (see Supplementary Information, Fig. S.1).

Concerning XRF analysis, the inhomogeneity of metal corrosion layers operates at two mutually interconnected levels. First, at the compositional level, demetallation (and eventually other processes) produces an in-depth variation of the percentages of the different elements. Second, at the 'physical' level, inhomogeneity is reflected in depth variations of the compaction, crystallinity, grain shape and size, and porosity of the corrosion layers. This second effect also influences XRF measurements, as conditions the penetration of the X-rays. Accordingly, and assuming that no X-ray absorption effects interfere, on sampling in different regions of the metal object, we obtain different elemental compositions. These can be taken as representative of the average composition of the region between the external surface and the depth reached by the X-rays in each measurement. In this scene, and according to experimental data (see below), as deeply X-rays penetrate until the metallic core, the measured elemental composition will increasingly approach the composition of the metal nucleus.

To reproduce experimental XRF data (see next section), let us assume that the sample is composed mainly of a noble metal M and a less noble metal M' accompanied by several minority components. In a given XRF measurement, the wt% of M and M' will be c_M and c_M', respectively. In the external layer of a binary alloy where M' is submitted to demetallation, the concentrations measured by XRF in different regions should vary as $c_M' = 100 - c_M$. Ideally, the plot of c_M' vs. c_M will be a straight line of slope − 1 that stops when the metal nucleus is reached. Then, $c_M' = c^\circ_M'$ and $c_M = c^\circ_M$, marking the endpoint of the above straight line in the c_M' vs. c_M plot.

Fig. 1 shows the wt% Zn vs. wt% Cu plot for surface XRF data recorded for a set of 18 brass statues from the Hofkirche in Innsbruck. Depending on the size and shape of the accessible metal surface 4–12 areas were measured on each statue. One can see that data points are grouped in an inclined band limited by the inclined straight line corresponding to an ideal binary alloy. Experimental data deviate from this ideal line due to the presence of minority components (Sn and Pb in particular). Additional components appear in the regions of the statues where the corrosion was more intensive (see Supplementary Information, Fig. S.2).

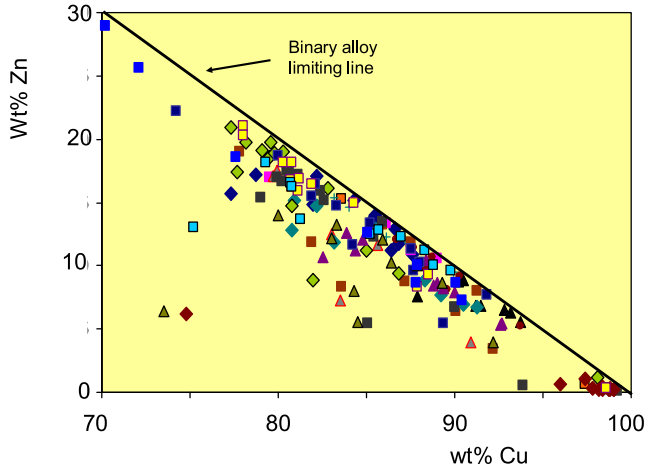

Fig. 1. Plots of wt% Zn vs. wt% Cu determined from surface XRF data for the studied brass statues from the Hofkirche in Innsbruck. The solid line corresponds to the theoretical line for the ideal demetallation of a binary metal composition. Error bars are omitted for simplicity.

As illustrated in Fig. 2 for HK01, XRF data for individual statues are grouped in tendency lines near to the above theoretical expectances. In this figure, we have depicted the idealized data corresponding to a binary 70 % Cu plus 30 % Zn brass and a ternary 80 % Cu, 10 % Z, 10 % Pb alloy where both Zn and Pb undergo demetallation. The endpoint of the respective c_M' vs. c_M (wt% Zn vs. wt% Cu) plots marks the composition of the metal nucleus. In the case of HK01, the composition of the alloy can be estimated as 80 % Cu, 18 % Zn, 2 % Pb.

Data such as in Fig. 2 permits the determination of the composition of the metal core of a metallic object submitted to selective demetallation from surface XRF measurements. However, accurate determination of the composition requires the fine determination of the endpoint of the c_M' vs. c_M graph. Since, in general, it cannot be easily accessible, a more detailed analysis of XRF data is needed. This requires the consideration of the mechanism of demetallation.

Corrosion with selective demetallation is a very complex process. It can be approached by considering that it has two basic characteristics: the involvement of phase transformations and the initiation in germs of quite small size. One of the ways to describe the time evolution of this type of system is to use solid-state reaction kinetics, in particular, the Avrami or Johnson-Mehl-Avrami-Erofeev-Kolmogorov (JMAEK) based Eqs. [18]. When describing an explicitly time-dependent phenomenon, the JMAEK equation corresponds to a sigmoidal function,

$$\alpha(t) = 1 - exp(-kt^m) \quad (1)$$

where $\alpha(t)$ represents the fraction of material that is transformed as a function of time, and k and m are constants that are extracted from the model. In solid-state reaction kinetics, k has the meaning of a rate constant of units (time)$^{-m}$ and m, the Avrami exponent ($m = 2$, 3, or 4, usually), is linked with the dimensionality of the system growth [22]. This equation can be generalized by replacing time by a quantityξ governing the evolution of the system so that m represents the dimensionality of the growth process in the α-ξ space [23]. For practical purposes, the JMAEK equation can be rewritten as,

$$[-ln(1-\alpha(\xi)]^{\frac{1}{m}} = b\xi \quad (2)$$

where $b = k^{1/m}$

In the case of selective demetallation which occurs during the corrosion of a binary metal alloy, the ratio c_M'/c_M can be used as a measure of the progress of the process. To unambiguously define a starting point, it is convenient to reformulate it as the inverse process defining the fractional conversion parameterα as the quotient between the actual c_M'/c_M ratio and the maximum ratio, c°_M'/c°_M, representative of the composition of the base alloy. Then, α can vary between 0 in regions of extreme demetallation (i.e., with entire loss of M') and 1 in regions where no demetallation has occurred. In turn, the driving parameterξ can be simply defined as $\xi = 100 - c_M$. Then, the variation of c_M'/c_M over c_M must follow a sigmoidal curve given by,

$$\left[-ln\left[1-\left(\frac{c_M'/c_M}{c^o_M'/c^o_M}\right)\right]\right]^{\frac{1}{m}} = b(100-c_M) \quad (3)$$

This equation can be linearized as,

$$ln\left[-ln\left[1-\left(\frac{c_M'/c_M}{c^o_M'/c^o_M}\right)\right]\right] = mlnb + mln(100-c_M) \quad (4)$$

In the following, we will use the (wt% Zn)/(wt% Cu) ($= f_{ZnCu}$) ratio as representative of the c_M'/c_M ratio in the previous theoretical

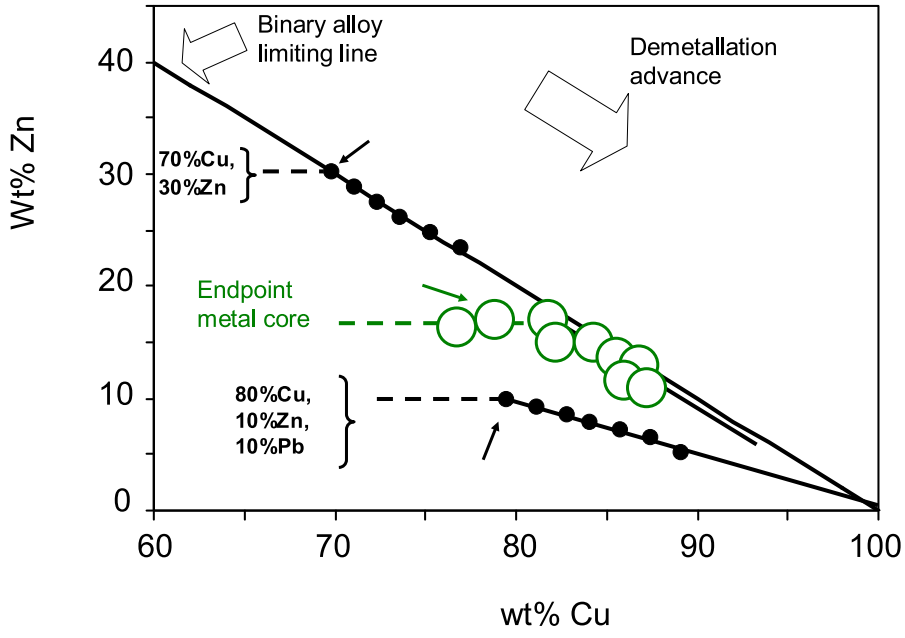

Fig. 2. Plots of wt% Zn vs. wt% Cu determined from surface XRF data for statue HK01 from the Hofkirche in Innsbruck (circles). Small solid circles correspond to the idealized data corresponding to a 70 % Cu plus 30 % Zn binary alloy and 80 % Cu, 10 % Z, 10 %Pb ternary alloy in which both Zn and Pb suffer demetallation. The continuous lines represent the ideal trend and the arrows mark the endpoints of the respective graphs. These define the Zn% of the respective metal core marked by horizontal dashed lines. From this graph, the composition of the metal nucleus of HK01 can be estimated as 80 % Cu, 18 % Zn, 2 % Pb.

treatment. Fig. 3 shows the (wt% Zn)/(wt% Cu) vs. wt% Cu plot of surface XRF data taken from different points of Hofkirche statues HK12 and HK14. Such data cover a relatively wide range of wt% Cu values indicating significant differences in the level of corrosion between the different areas of the statues. XRF data appear to define two distinct lines of tendency which, in principle, can be approximated to saturation, s-shaped curves where f_{ZnCu} tends to a plateau. This plateau corresponds to the limiting Zn to Cu ratio, f^{lim}_{ZnCu}, that can be taken as the Zn/Cu ratio in the base metal alloy.

Experimental data can be fitted reasonably to the above theoretical model. Fig. 4 shows the plots of $\ln[-\ln(1-f_{ZnCu}/f^{lim}_{ZnCu})]$ vs. ln(100-wt% Cu) from experimental XRF data recorded in statues HK01 and HK21 in both cases taking $f^{lim}_{ZnCu} = 0.225$ and $f^{lim}_{ZnCu} = 0.150$ respectively. Despite relatively large data dispersion, experimental XRF data can be approximated satisfactorily to straight lines in agreement with the predictions from Eq. (4). The slope of such lines is the same within the range of uncertainty (2.1 ± 0.3 for HK01 and 2.0 ± 0.3 for HK21), corresponding to the JMAEK modeling with $m = 2$. The values of the constant b can be calculated from the intercepts (-5.5 ± 0.9 for HK01 and -4.7 ± 1.2 for HK21) as $0.07(5) \pm 0.03$ and $0.09(5) \pm 0.04$ (wt% Cu)$^{-1}$.

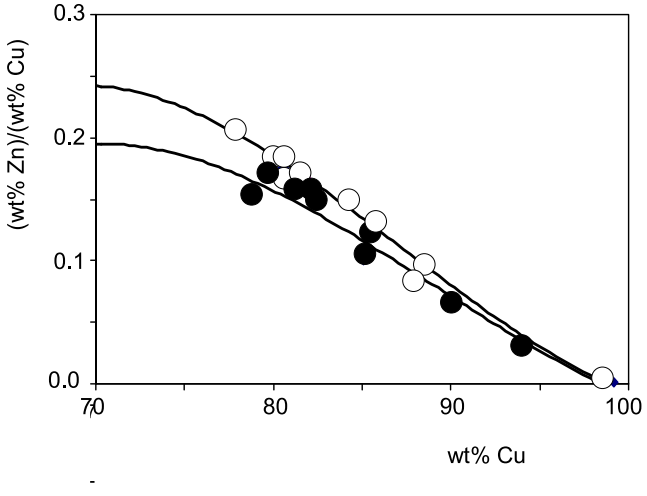

Fig. 3. Plots of f_{ZnCu} (= (wt% Zn)/(wt% Cu)) vs. wt% Cu plots for statues HK05 (squares), HK12 (solid circles), and HK14 (circles) from surface XRF data. Error bars are omitted for simplicity. Continuous lines are 3rd-degree polynomial functions.

This methodology permits the estimate of the composition of the metal alloy from the values of f^{lim}_{ZnCu}. Since it requires the aid of linear representations such as in Fig. 3, a minimum number of 5–7 data points is required. The data obtained for the 18 studied statues are listed in Table S.1 (Supplementary Information). Interestingly, such data exhibit a relative heterogeneity not only in the f^{lim}_{ZnCu} but also in the values of the JMAEK parameters m and b. These differences can reflect differences in the composition, manufacturing procedure, and corrosion history. Eventually, such differences could reflect the differences in the fabrication 'habit' of different workshops and applied to characterize it.

4. Conclusions

Examination of surface XRF data for various binary and non-binary historical brass and bronze objects suggests that the corrosion process is generally accompanied by a loss of the less noble components (Zn, Sn, Pb) relative to Cu. This demetallation process can be described in terms of Johnson-Mehl-Avrami-Erofeev-Kolmogorov (JMAEK) type equations, using the less noble metal/noble metal mass ratio as a quantity representing the fractional reaction advance. The JMAEK-type equations predict sigmoidal variations of this ratio with noble metal concentration, the plateau of which determines the composition of the metal core.

The method has been applied to surface XRF data from early 16th-century Renaissance brass statues from the Hofkirche in Innsbruck, Austria, allowing for the determination of the composition of the respective metal nuclei.

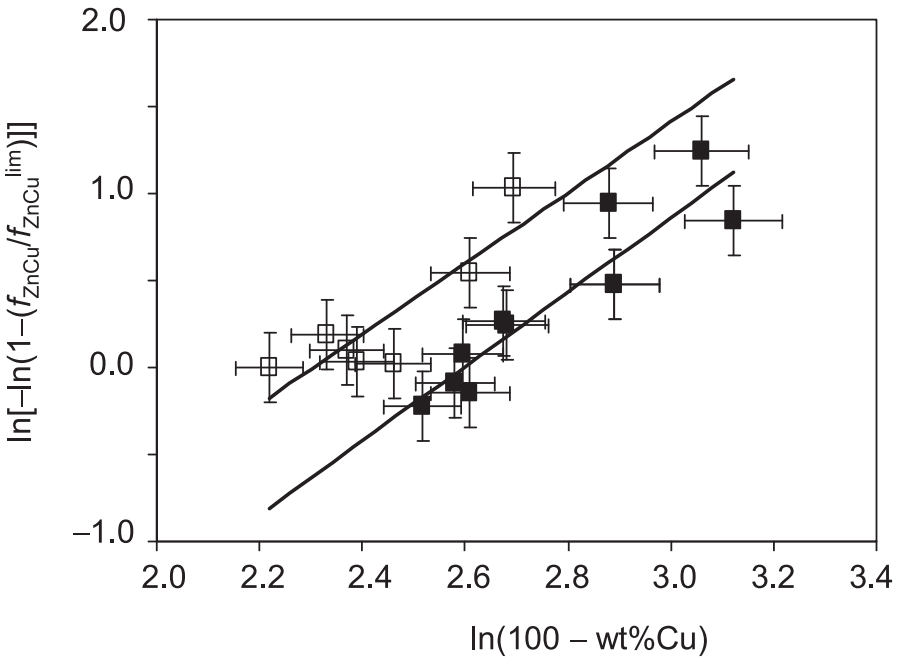

Fig. 4. ln[−ln(1-f_{ZnCu}/f^{lim}_{ZnCu})] vs. ln(100-wt% Cu) plots from experimental XRF data recorded in statues HK01 (solid squares) and HK21 (squares). The solid lines correspond to the linear fit of experimental data.

CRediT authorship contribution statement

Antonio Doménech-Carbó: Writing – original draft, Formal analysis, Conceptualization. **Marianne Mödlinger:** Writing – review & editing, Funding acquisition, Data curation. **Giorgia Ghiara:** Data curation.

Declaration of competing interest

The authors declare no existing competing interests.

Data availability

Data will be made available on request.

Acknowledgements

Project P34960-G supported by the Austrian Science Fund (FWF), project PID2020-113022GB-I00 supported by MCIN/AEI/10.13039/501100011033, Fondo Europeo de Desarrollo Regional (ERDF) and Agencia Estatal de Investigación (AEI), and Project AICO/2021/095 which is supported with Generalitat Valenciana and Fondo Europeo de Desarrollo Regional (ERDF), funds are gratefully acknowledged. This research was funded in part also by the Austrian Science Fund (FWF) [10.55776/ P 34960-G]. The XRF analyses were carried out by researchers of the CNR-IBE S. Michele all'Adige (Trento, Italy) (M. Negri, M. Fellin, J. Bontadi) with an Oxford Instruments X-MET5100 instrument with a high resolution detector. For the purpose of open access, the author has applied a CC BY public copyright licence to any Author Accepted Manuscript version arising from this submission.

Appendix A. Supplementary data

Supplementary data to this article can be found online at https://doi.org/10.1016/j.sab.2024.107030.

References

[1] P. Holakooei, O. Oudbashi, M. Mortazavi, M. Ferretti, On, under and beneath the patina: evaluation of micro energy dispersive X-ray fluorescence quantitative data on the classification of archaeological copper alloys, Spectrochim. Acta B At. Spectrosc. 178 (2021) 106128.
[2] J.M. Del Hoyo-Meléndez, M. Matosz, A. Walanus, P. Krupska-Wolas, Advantages and limitations of archaeometric analysis of archaeological metals: a focus on statistical methods applied to portable XRF spectrometry data, Microchem. J. 51 (2023) 104156.
[3] P. Moioli, C. Seccaroni, Analysis of art objects using a portable x-ray fluorescence spectrometer, X-Ray Spectrom. 29 (2000) 48–52.
[4] M. Ferretti, The investigation of ancient metal artefacts by portable X-ray fluorescence devices, J. Anal. At. Spectrom 29 (2014) 1753–1766.
[5] S. Porcinai, A. Cagnini, M. Galeotti, M. Ferretti, Quantitative analysis of copper alloys by means of portable X-ray fluorescence: a comparison between analysis of shavings and surfaces, Spectrochim. Acta B At. Spectrosc. 210 (2023) 106808.
[6] A. Bolewski, M. Matosz, W. Pohorecki, J.M. del Hoyo-Meléndez, Comparison of neutron activation analysis (NAA) and energy dispersive X-ray fluorescenc spectrometry for the non-destructive analysis of coins minted under the early Piast dynasty, Radiat. Phys. Chem. 171 (2020) 108699.
[7] R. Jenkins, R.W. Gould, D. Gedcke, Quantitative X-Ray Spectrometry, 2nd Edit, Marcel Dekker, New York, 1995.
[8] D. Šatović, V. Desnica, S. Fazinić, Use of portable X-ray flourescence instrument for bulk alloy analysis on low corroded indoor bronzes, Spectrochim. Acta B At. Spectrosc. 89 (2013) 7–13.
[9] A. Heginbotham, V.A. Solé, CHARMed PyMca, part I: a protocol for improved inter-laboratory reproducibility in the quantitative ED-XRF analysis of copper alloys: CHARMed PyMca, part 1, Archaeometry 59 (2017) 714–730.
[10] A. Heginbotham, D. Bourgarit, J. Day, J. Dorscheid, J. Godla, L. Lee, A. Pappot, D. Robcis, CHARMed PyMca, part II: an evaluation of interlaboratory reproducibility for ED-XRF analysis of copper alloys, Archaeometry 61 (2019) 1333–1352.
[11] I. Constantinides, A. Adrianes, F. Adams, Surface characterization of artificial corrosion layers on copper alloy reference materials, Appl. Surf. Sci. 189 (2002) 90–101.
[12] A. Heginbotham, J. Bassett, D. Bourgarit, C. Eveleigh, L. Glinsman, D. Hook, D. Smith, R.J. Speakman, A. Shugar, R. Van Langh, The copper CHARM set: a new set of certified reference materials for the standardization of quantitative X-ray fluorescence analysis of heritage copper alloys*: the copper CHARM set, Archaeometry 57 (2015) 856–868.
[13] B. Moeini, H. Haack, F.N. Neal, V. Fernandez, T.R. Gengenbach, C.D. Easton, M. R. Linford, Box plots: a simple graphical tool for visualizing overfitting in peak fitting as demonstrated with X-ray photoelectron spectroscopy data, J. Electron Spectrosc. Relat. Phenom. 250 (2021) 147094.
[14] T. Kohonen, Essentials of the self-organizing map, Neural Netw. 37 (2013) 52–65.

[15] V.A. Solé, E. Papillon, M. Cotte, Ph. Walter, J. Susini, A multiplatform code for the analysis of energy-dispersive X-ray fluorescence spectra, Spectrochim. Acta B At. Spectrosc. 62 (2007) 63–68.
[16] N.D. Meeks, Tin-rich surfaces on bronze – some experimental and archaeological considerations, Archaeometry 28 (1986) 133–162.
[17] C. Chiavari, K. Rahmouni, H. Takenouti, S. Joiret, P. Vermaut, L. Robbiola, Composition and electrochemical properties of natural patinas of outdoor bronze monuments, Electrochim. Acta 52 (2007) 7760–7769.
[18] F.J. Gotor, J.M. Criado, J. Malek, N. Koga, Kinetic analysis of solid-state reactions: the universality of master plots for analyzing isothermal and nonisothermal experiments, J. Phys. Chem. A 104 (2000) 10777–10782.
[19] M. Mödlinger, B. Asmus, G. Ghiara, The "Schwarze Mander" of the court church in Innsbruck, Austria: manufacture and production of monumental brass statues in the renaissance, Int. J. Metal Cast. (2024), https://doi.org/10.1007/s40962-024-01299-4.
[20] M. Mödlinger, M. Bernabei, J. Bontadi, M. Fellin, M. Fera, G. Ghiara, M. Negri, J. Utz, Multidisciplinary analyses on the 11th–12th century bronze doors of san Marco, Venice, PloS One 18 (2013) e0288094.
[21] M. Mödlinger, J. Bontadi, M. Fellin, M. Fera, M. Negri, J. Utz, G. Ghiara, The medieval bronze doors of san Zeno, Verona: combining material analyses and art history, Herit. Sci. 12 (2024) 26.
[22] K. Dimitra, C. Konstantinos, Nonisothermal crystallization kinetics: studying the validity of different Johnson–Mehl–Avrami–Erofeev–Kolmogorov (JMAEK) based equations, Themochim. Acta 704 (2021) 179030.
[23] A. Doménech-Carbó, Exploring nucleation modeling of the voltammetry of solid-to-solid state redox processes with phase changes, J. Solid State Electrochem. 28 (2024) 1497–1507.